Synthesis and physical properties of the 10.6 K ferromagnet $NdIr_3$

Karolina Górnicka,[1] Weiwei Xie,[2] Elizabeth M. Carnicom,[3] Robert J. Cava,[3] and Tomasz Klimczuk[1]
[1]*Faculty of Applied Physics and Mathematics, Gdansk University of Technology, ul. Narutowicza 11/12, 80-233 Gdańsk, Poland*
[2]*Department of Chemistry, Louisiana State University, Baton Rouge, Louisiana 70803, USA*
[3]*Department of Chemistry, Princeton University, Princeton, New Jersey 08544, USA*

(Received 5 November 2018; revised manuscript received 2 January 2019; published 26 March 2019)

The magnetic, transport, and thermodynamic properties of $NdIr_3$ are reported. Its $PuNi_3$-type crystal structure (space group R-3m), with lattice parameters $a = 5.3262(1)$ Å and $c = 26.2218(3)$ Å, was confirmed by powder x-ray diffraction. Our measurements indicate that $NdIr_3$ exhibits a previously unreported paramagnetic to ferromagnetic phase transition below $T_C = 10.6$ K (determined by using the Arrott plot). The magnetic susceptibility obeys the Curie-Weiss law with an effective magnetic moment of $\mu_{\text{eff}} = 3.63(2)\ \mu_B$/Nd and a paramagnetic Curie temperature $\theta_P = 5.4(6)$ K. The heat-capacity anomaly at T_C confirms a bulk nature of the transition, though $\Delta C_p = 11.7\,\text{J mol}^{-1}\,\text{K}^{-1}$ is lower than expected for $J = 9/2$ and instead close to the $J = 1/2$ system. This suggests that Nd ions are subject to the crystalline electrical field that removes spin degeneracy and leaves the Nd ions in a doublet ground state. Resistivity and heat-capacity measurements reveal an anomaly at around 70 K. The origin of this anomaly is unknown, but the lack of thermal hysteresis suggests that it is a second-order phase transition and may be related to electronic instabilities. The calculated electronic structure is reported.

DOI: 10.1103/PhysRevB.99.104430

I. INTRODUCTION

Intermetallic compounds based on rare-earth (RE) and transition metals (T) have been and remain of considerable interest in many fundamental and industrial studies [1–7]. RE-T binary phase diagrams are generally rather complex with multiple eutectics and include compounds with both high and low melting temperatures—characteristics that can inhibit obtaining pure phases and determining their structures. In general, the RE richest binary compounds form in the cementite crystal structure type (RE_3T). It has been reported in several cases that long-range magnetic ordering originates from the RE atoms, while the T atoms are nonmagnetic [8–12]. The lack of magnetism for the T atoms in this structure type is one of the reasons why the nonmagnetic rare-earth variants, La_3Co and La_3Ni, display superconducting ground states with $T_c = 4.5$ and 6 K, respectively [13,14].

The light rare-earth RE-T phase diagrams have been well studied only for the 3d transition elements Co and Ni and the 4d T element Ru. The compounds formed are an important class of materials exhibiting a variety of physical phenomena, like superconductivity [15–21] and different types of magnetic ordering [22–27]. Among them, binary compounds of the RET_5, RE_2T_7, RET_3, and RET_2 types, where RE is a light lanthanide metal, have been extensively studied [15,22,28–30]. All these compounds belong to a $RE_{2m+n}T_{4m+5n}$ homologous series, where m and n represent the number of $MgCu_2$- and $CaCu_5$-type blocks, respectively. For example, $m = 0$ and $n = 1$ give RET_5, which is the richest T compound in the series. In a similar manner a Laves phase (RET_2) is obtained for $m = 1$ and $n = 0$ [31–34].

In spite of numerous experimental studies of RET_3 compounds with T = Co and Ni [35–41], there are limited reports for systems focused on the Ir- or Rh-rich materials, even though, especially for the case of Ir, the spin-orbit coupling of the d element is likely to influence the magnetic properties. This is most probably caused by difficulties in the synthesis of these binaries. In this respect, compounds containing Ir and RE metals have not been widely investigated—information about physical properties is available only for $LaIr_3$ [42] and $CeIr_3$ [43], compounds that display superconducting behavior. The crystal structures for the $PrIr_3$, $NdIr_3$, $GdIr_3$, YIr_3, and $ScIr_3$ binaries [44–46] have been reported, but no further characterization is available. Thus, we report here on the magnetic, thermal, and transport properties of $NdIr_3$, characterizing its ferromagnetic (FM) state with a Curie temperature $T_C = 10.6$ K. Its calculated electronic structure is also reported.

II. EXPERIMENTAL DETAILS

The polycrystalline sample of $NdIr_3$ was prepared by melting the required high-purity elements, i.e., Nd (99.99%) and Ir (99.9%), under an argon atmosphere inside an arc-melting furnace (MAM-1 Edmund Buhler GmbH). A piece of zirconium was used as a getter material during the melting process. The expected loss of Nd was compensated by adding a carefully assigned extra amount of Nd (∼1% total mass). After the initial melt, the sample button was turned and remelted three times to improve reaction among the constituents. The weight loss upon melting was lower than 0.5%. The obtained sample was then wrapped in tantalum foil and heat treated at 1350 °C for 36 h under high vacuum (10^{-5} torr). Subsequently, the resulting material was powderized, pressed into a pellet, and then annealed under high vacuum at 1370 °C for 36 h. No melting was observed and the resulting material was hard and dense.

The structure and phase purity of the annealed sample was checked at room temperature by powder x-ray diffraction

(pXRD) on a Bruker D8 Advance Eco diffractometer with Cu Kα radiation and a LynxEye-XE detector. The fullprof package was used for Rietveld fitting of the pXRD data [47]. A Quantum Design Dynacool Physical Property Measurement System (PPMS) with a vibrating sample magnetometer function was used to measure the field-dependent magnetization at 2 K and the temperature-dependent magnetic susceptibility (defined as dM/dH where M is the magnetization and H is the applied field). The temperature dependencies of the zero-field cooled (ZFC) and field cooled (FC) magnetizations were measured in applied fields of 1, 10, and 100 mT. Magnetic measurements were performed on a sample of arbitrary shape with a mass of about 30 mg.

The temperature dependences of electrical resistivity and heat capacity were performed using a PPMS Evercool II. The resistivity was determined using a standard four-probe technique, with four 37-μm-diameter platinum wire leads spark-welded to the flat polished sample surface. Specific-heat measurements were measured in zero field and field up to 3 T, using the two-τ time-relaxation method.

The electronic structure, including the density of states (DOS) and band structure of $NdIr_3$, was calculated by the tight-binding linear muffin-tin orbital method in the atomic sphere approximation using the stuttgart code [48]. Exchange and correlation were treated by the local-density approximation [49]. The $4f$ electrons on Nd were treated as core electrons [50]. The basis set for the calculations included the following wave functions: Nd $6s$, $6p$, and $5d$ and Ir $6s$, $6p$, and $5d$. The convergence criterion was set to 0.5 meV. A mesh of $8\times8\times8$ k points in the irreducible wedge of the first Brillouin zone was used to obtain all integrated values, including the DOS and band structure [51].

III. RESULTS AND DISCUSSION

The room-temperature pXRD pattern together with the Rietveld refinement is presented in Fig. 1. Ning *et al.* [52] reported that $NdIr_3$ forms in the $AuCu_3$-type cubic structure with $a = 3.836$ Å. However, Blazina *et al.* [44] proposed that this binary compound belongs to the rhombohedral branch of the homologous series described above. Our pXRD analysis confirms the latter structure for our material—all the diffraction peaks correspond to the rhombohedral crystal structure

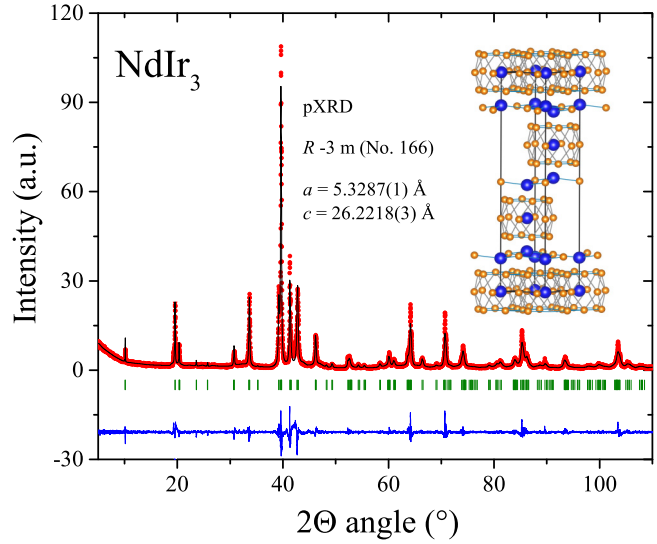

FIG. 1. Powder x-ray-diffraction pattern of $NdIr_3$ (red points) together with the Rietveld refinement profile (black solid line). The blue curve is the difference between experimental and model results. The green vertical bars indicate the expected Bragg peak positions (space group R-3 m). Inset: The $NdIr_3$ crystal structure, with Nd and Ir atoms represented by blue and orange balls, respectively.

(space group R-3 m, no. 166). The refined atomic coordinates together with selected interatomic distances, all of which are defined to very good precision, are gathered in Table I. The unit cell contains two and three crystallographically inequivalent Nd and Ir sites, respectively. The crystal structure of $NdIr_3$ is shown in the inset of Fig. 1. It consists of blocks of truncated icosahedra formed by Ir2 and Ir3 atoms centered by Nd1 atoms. These blocks are separated by hexagonal layer build by Nd2 and Ir1 atoms.

The difference plot (between experimental and fitted data) and the Bragg positions are also shown in Fig. 1. $NdIr_3$ was found to be a single phase with no extra peaks corresponding to any detectable impurities or secondary phase. The lattice parameters obtained from the Rietveld profile refinement are $a = 5.3287(1)$ Å and $c = 26.2218(4)$ Å. Whereas the a-lattice parameter is similar to that previously reported for $NdIr_3$ [44], the c-lattice parameter is about 1% larger ($c = 25.998$ Å in

TABLE I. Refined structural parameters for $NdIr_3$ and selected interatomic distances d in angstroms. Space group R-3 m (166), $a = 5.3287(1)$ Å, and $c = 26.2218(4)$ Å. B_{iso} is the thermal displacement parameter in square angstroms. Background-corrected Rietveld refinement reliability factors: profile residual $R_p = 20.8\%$, weighted profile residual $R_{WP} = 19.9\%$, expected residual $R_{exp} = 6.8\%$, goodness of fit $\chi^2 = 2.8$.

Atom	Wyck.	Occ.	x	y	Z	B_{iso}(Å^2)
Nd1	3a	1	0	0	0	1.12(6)
Nd2	6c	1	0	0	0.1510(2)	0.93(2)
Ir1	3b	1	0	0	½	0.85(9)
Ir2	6c	1	0	0	⅓	0.55(8)
Ir3	18h	1	0.4972(4)	0.5028(3)	0.0824(1)	0.71(5)
Nd1-Ir2 (×6)		3.071		Nd2-Ir1 (×3)		3.104
Nd1-Ir3 (×12)		3.430		Nd2-Ir3 (×3)		3.052
				Nd2-Ir3 (×6)		3.215

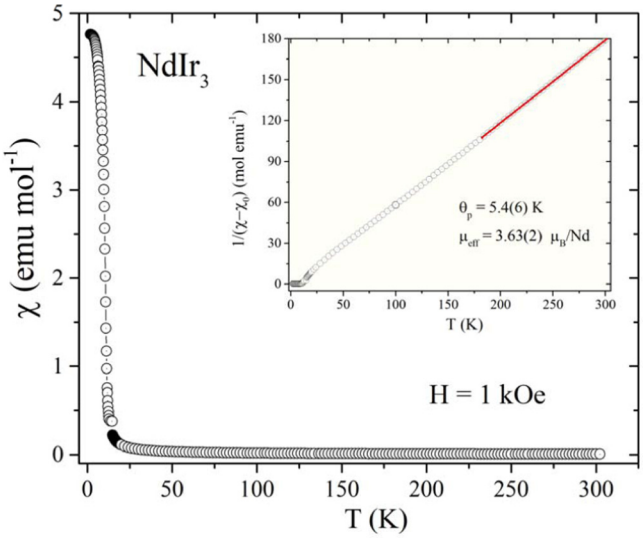

FIG. 2. Temperature dependence of the ZFC magnetic susceptibility $\chi(T)$ in a field of 1000 Oe. Inset: The reciprocal susceptibility vs temperature. The red solid line represents a fit to the modified Curie-Weiss law.

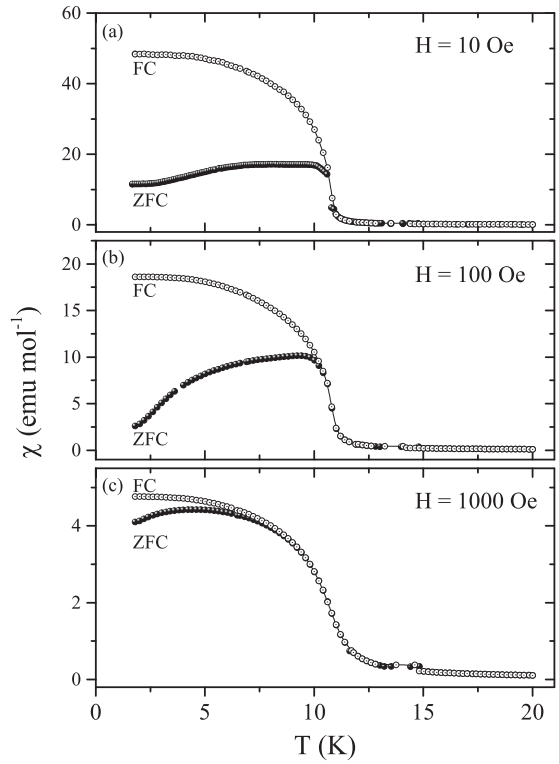

FIG. 3. The difference between FC and ZFC magnetic susceptibility $\chi(T)$ of $NdIr_3$ in the temperature range of 1.9–20 K under applied magnetic fields of (a) 10 Oe, (b) 100 Oe, and (c) 1000 Oe.

the previous study [44]). The Rietveld refinement gives a moderately high χ^2 value ($\chi^2 = 2.8$) due to the difficulty in fitting the observed peak shapes with standard functions, likely related to a strain distribution or defects, e.g., stacking faults, within the material [53]. Nonetheless the material is very clearly single phase with a well-defined rhombohedral structure as described above.

The magnetization of $NdIr_3$ was measured and analyzed in detail. The temperature dependence of the magnetic susceptibility of $NdIr_3$ measured in an applied field of 0.1 T is displayed in Fig. 2. In the low-temperature region, the susceptibility abruptly increases, suggesting a transition into a ferromagnetic state. The inset of Fig. 2 presents the reciprocal susceptibility $1/(\chi-\chi_0)$ versus temperature. Between 175 and 300 K, the experimental data were fitted by the modified Curie-Weiss law ($R^2 = 0.9999$), $\chi = \chi_0 + C/(T-\theta_P)$, where C and θ_P are the Curie constant and the paramagnetic (PM) Curie temperature, respectively. The temperature independent susceptibility term $\chi_0 = 4.9(2) \times 10^{-5}$emu mol^{-1} and comes from both the sample and a sample holder. The fit, shown by the red solid line, gave $C = 1.65(1)$ emu K and $\theta_P = 5.4(6)$ K. Having the Curie constant, and assuming that the magnetic moment originates from Nd^{3+} only, the effective magnetic moment per Nd can be obtained using the relation $\mu_{\text{eff}} = (\frac{3Ck_B}{\mu_B^2 N_A})^{1/2}$, where k_B is the Boltzmann constant, μ_B is the Bohr magneton, and N_A is Avogadro's number. The resulting effective magnetic moment for $NdIr_3$ deduced from the paramagnetic region is 3.63(2) μ_B/Nd and is very close to the expected value for the free Nd^{3+} ion ($\mu_{\text{eff}} = 3.62\mu_B$) [54]. The positive paramagnetic Curie temperature, $\theta_P = 5.4(6)$ K, indicates the presence of dominantly ferromagnetic interactions within the paramagnetic state.

Figure 3 displays the magnetic susceptibility of $NdIr_3$ taken as a function of temperature in a constant magnetic field of (a) 10 Oe, (b) 100 Oe, and (c) 1000 Oe. Even at the lowest applied magnetic field (10 Oe), below 11 K a sudden increase of $\chi(T)$ is observed, suggesting a ferromagnetic ground state [54–60]. The transition temperature, estimated as the minimum of $d\chi/dT$ for $H = 10$ Oe, is about 10.6 K. The magnetic susceptibility is strongly dependent on the magnetic history of the sample; i.e., below a certain temperature, ZFC and FC $\chi(T)$ curves exhibit a significant irreversibility which starts to disappear for magnetic fields larger than 1000 Oe [Fig. 3(c)]. The observed bifurcation can be attributed to the domain-wall pinning effect associated with a hysteresis loop (Fig. 4) as a consequence of the magnetocrystalline anisotropy [54,56]. We also measured the magnetic susceptibility in higher magnetic fields: 0.5, 1, and 1.5 T. The results obtained were used to calculate the transition temperature in different magnetic fields and to draw the border line for a tentative magnetic phase diagram (see below).

As a further characterization of the magnetic ground state in $NdIr_3$, Fig. 4 presents the field-dependent magnetization measured at $T = 2$ K. As shown in the inset of Fig. 4, the $M(H)$ dependence is characteristic of a ferromagnetic material. The rather narrow hysteresis loop ($H_{\text{coercive}} = 380$ Oe) may indicate that $NdIr_3$ is a soft ferromagnet with a remnant magnetization ($\mu_R = 0.6\mu_B$/Nd) being over 35% of the magnetization at 9 T. Although the $M(H)$ curve shows a tendency to a constant value, the magnetization reaches about $1.7\mu_B$ by $\mu_0 H = 9$ T, which is lower than the expected saturated value for Nd^{3+} ($\mu_S = gJ = 3.27\mu_B$, where J is the total angular momentum and g is the Landé g factor [54]). The lower than full value of the magnetization at 9 T may be attributed to the effect of the crystalline electric-field (CEF) splitting of the Nd

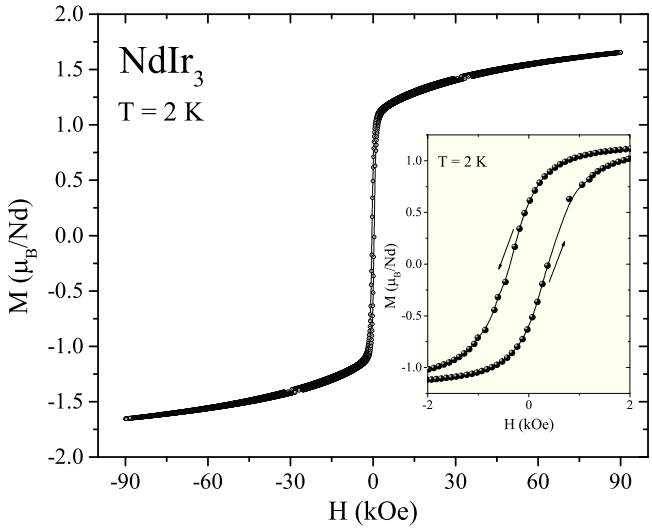

FIG. 4. The isothermal magnetization M as a function of magnetic field measured for $NdIr_3$ at 2 K. Inset: The low-field part on an expanded scale.

magnetic levels [54,61,62], a random distribution of the hard and easy magnetization axes of the grains that compose the polycrystalline sample [63], or the fact that a higher applied field is necessary to reach the full saturated moment.

The occurrence of the ferromagnetic state for $NdIr_3$ may be confirmed by a comparison of the magnetic isotherms plotted in the form of M^2 versus H/M (i.e., Arrott plots [64,65]). It is expected that for ferromagnetic materials the high-field isotherms are parallel lines, and that the isotherm at the Curie temperature will pass through the origin [66–70]. For $NdIr_3$ such curves indicate that ferromagnetic ordering occurs at a temperature slightly above 10.5 K as the intercept of the linear fit to the M^2 versus H/M curve is closest to (0,0) (Fig. 5) for that temperature. As seen from Fig. 5, for $T < T_C$, a downturn of the Arrott plots in low

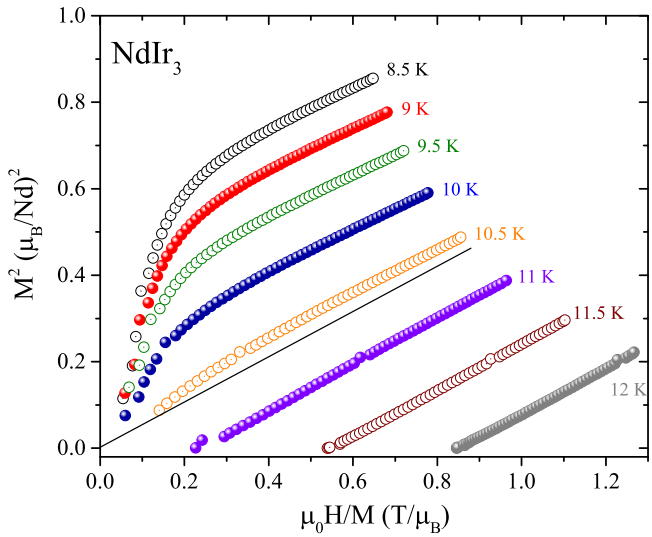

FIG. 5. Arrott plots for $NdIr_3$. The solid line is used to estimate the Curie temperature.

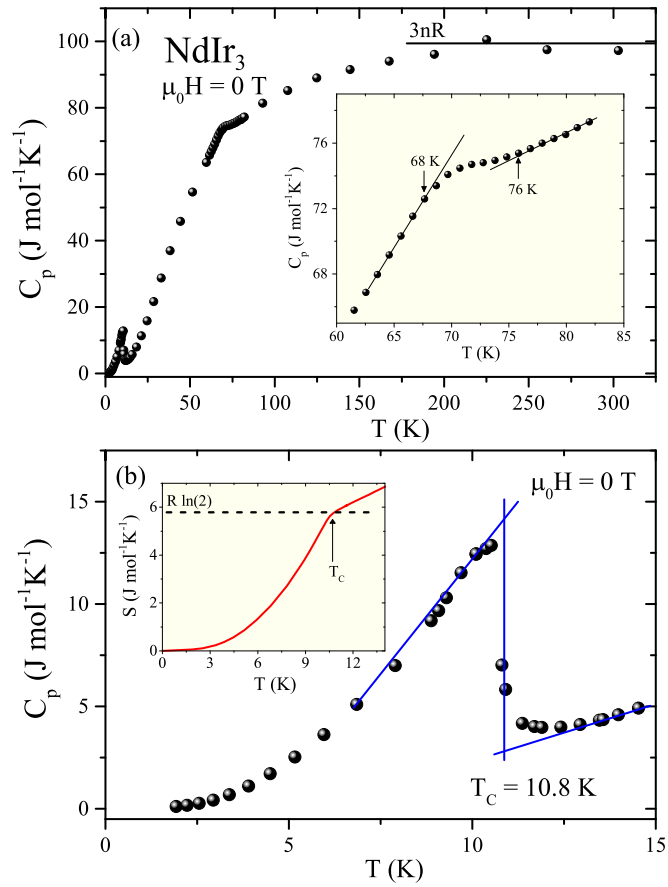

FIG. 6. (a) The temperature dependence of the specific heat $C_p(T)$ of $NdIr_3$ measured in the temperature range 1.95–300 K. Inset: The expanded view of the high-temperature transition. (b) The specific-heat anomaly in zero magnetic field at low temperatures. Inset: The entropy $S(T)$ of $NdIr_3$. The arrow indicates the FM ordering temperature.

magnetic fields is noticed. Such behavior is observed frequently and can be explained as a result of a magnetocrystalline anisotropy or the presence of a metamagnetic transition at low temperature [55–57,66]. The linear behavior of the isotherms in high fields indicates the presence of mean-field interactions [66].

Further information on the magnetic properties of $NdIr_3$ can be gained from specific-heat measurements. The main panel of Fig. 6(a) depicts the temperature dependence of the zero-field specific heat C_p from 1.95 to 300 K. At room temperature, C_p is close to the expected value calculated from the Dulong-Petit law $3nR \approx 100\,\mathrm{J\,mol^{-1}K^{-1}}$, where $n = 4$ is the number of atoms per formula unit and $R = 8.314\,\mathrm{J\,mol^{-1}K^{-1}}$ is the gas constant. At low temperature, $NdIr_3$ exhibits a clear λ-like anomaly, which can be attributed to a second-order phase transition of magnetic origin. In addition to the distinct ferromagnetic transition near 11 K, the thermodynamic data show a clear feature between 68 and 76 K [inset Fig. 6(a)]. The broad shape of the observed anomaly indicates that the transition is also second order. A dramatic structural transition [56,71,72] is therefore excluded, but there may be a transition to a closely related polymorph [73] or

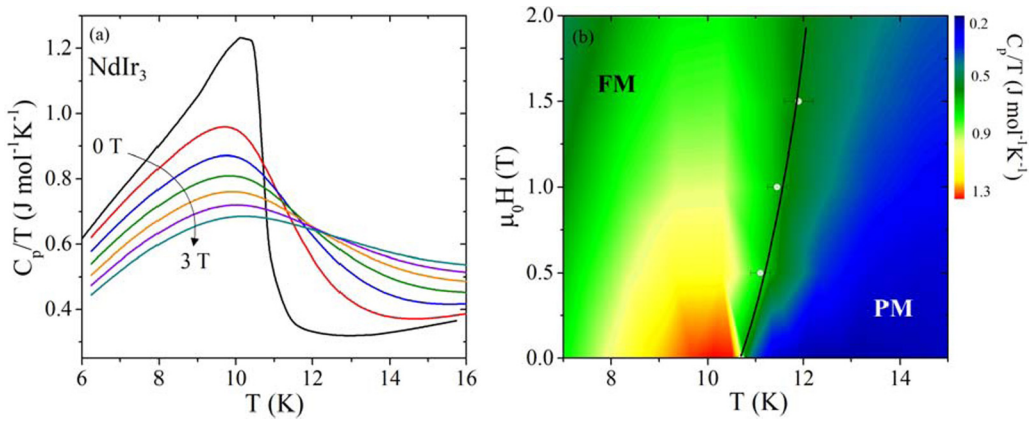

FIG. 7. (a) The dependence of the specific heat C_p on temperature in applied magnetic fields $\mu_0 H$ up to 3 T. (b) Map of the specific heat of $NdIr_3$ as a function of temperature and applied magnetic field.

the formation of a charge-density wave (CDW). The calculated entropy associated with this transition is $S = 0.04R$, which is much smaller than reported for $RE_5Ir_4Si_{10}$ CDW compounds [74–76]. Figure 6(b) shows the heat capacity of $NdIr_3$ in a zero applied magnetic field around the magnetic ordering temperature. In order to calculate the value of the specific-heat jump, we used a linear approximation of the data just above and below the transition for the background. The corresponding graphical construction with the vertical line located at the transition temperature ($T_C = 10.8$ K) is shown by solid blue lines. For a mean-field-like FM transition, the expected value for the specific-heat jump of a $J = 9/2$ Heisenberg system is equal to $\Delta C_p = 20.4\,\mathrm{J\,mol^{-1}K^{-1}}$, where $\Delta C_p = N \times 5R[J(J+1)/(2J^2+2J+1)]$ [56], where $N = 1$ is the number of RE atoms per mole. In contrast, the specific-heat jump of $NdIr_3$ is found to be only about $11.7\,\mathrm{J\,mol^{-1}K^{-1}}$. Assuming $J = 1/2$, the calculated specific jump is $\Delta C_p = 12.5\,\mathrm{J\,mol^{-1}K^{-1}}$, which is very close to the experimental value and may indicate that the CEF removes the spin degeneracy and leaves the Nd ions in a doublet ground state.

The entropy of $NdIr_3$ was inferred by integrating C_p/T and is presented in the inset of Fig. 6(b). At the Curie temperature (T_C), the entropy reaches about 98% of $R\ln(2)$, which is expected for the doublet ground state, again confirming that CEF reduces the spin degeneracy in $NdIr_3$. In another scenario, only a fraction of the Nd ions may be involved in magnetic ordering [54,56]. In order to characterize the low-temperature magnetic transition in more detail, neutron diffraction, which is beyond the scope of the present paper, would be of interest.

Figure 7(a) presents the low-temperature part of the thermodynamic data for $NdIr_3$ in applied magnetic fields up to 3 T. With increasing external magnetic field, the magnetic phase transition exhibits a gradual weakening and shifting to higher temperatures. This is typical behavior for ferromagnetic materials [54,55,60]. In Fig. 7(b), a map of the specific heat of $NdIr_3$ as a function of temperature and applied magnetic field (up to $\mu_0 H = 2\,T$) is depicted. The phase boundary between the PM and FM states (black line) was deduced based on the transition temperatures (open circles) determined as the minimum of $d\chi/dT$ at each applied magnetic field $\mu_0 H = 0$, 0.5, 1, and 1.5 T.

The temperature dependence of the electrical resistivity $\rho(T)$ is shown in Fig. 8. The measurement was performed in zero magnetic field in the temperature range from 1.85 K to room temperature. The resistivity curve exhibits metallic character ($d\rho/dT > 0$) with slightly curvilinear behavior that suggests that some additional scattering processes, e.g., Mott interband scattering, determine the electrical resistivity of $NdIr_3$ at ambient temperature [54,60,77]. The resistivity at room temperature is about 370 $\mu\Omega$ cm. This is a large value for a metallic system although still in the metallic range [78]. A similar value of the electrical resistivity at ambient temperature is observed for PrPtIn [77]. The plotted curve shows a feature near 70 K, consistent with the anomaly observed in the specific-heat data (inset Fig. 8). It is worthwhile to note that a detailed analysis of the heating-cooling curve (not shown here) does not reveal any discernible hysteresis loop, which would be expected for a first-order phase transition [71,72]. It was also found that the resistance anomaly does

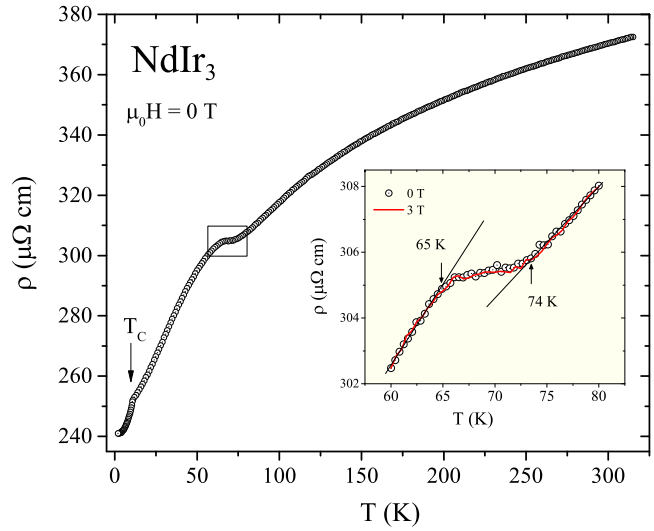

FIG. 8. The temperature dependence of the electrical resistivity for $NdIr_3$ between 1.85 and 300 K in zero magnetic field. Inset: Expanded view of the high-temperature anomaly. The red solid line represents data obtained in an applied field of 3 T.

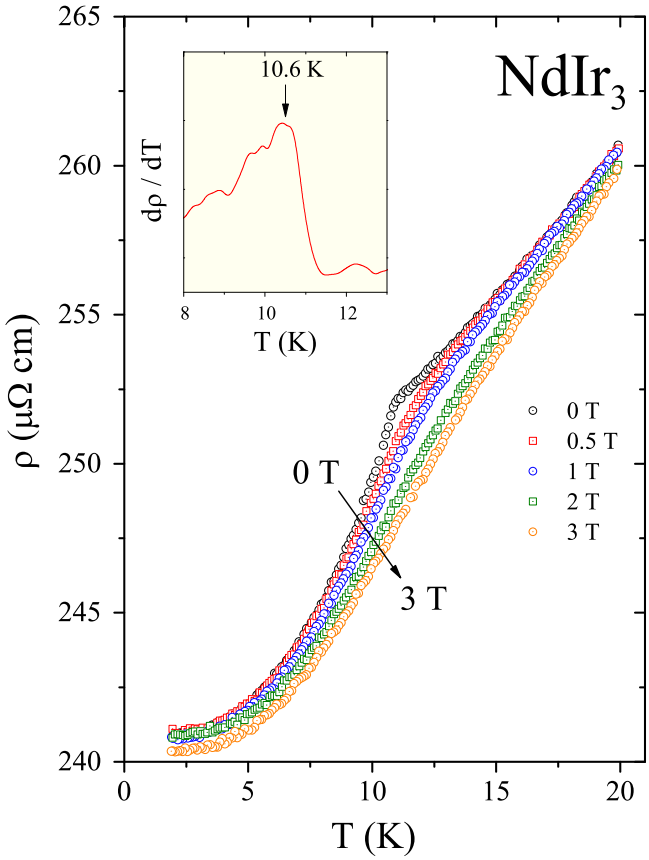

FIG. 9. Temperature-dependent electrical resistivity $\rho(T)$ for $NdIr_3$ in zero magnetic field and in applied magnetic fields up to 3 T in the vicinity of the transition. Inset: $d\rho/dT$ vs temperature around the magnetic transition in zero applied field.

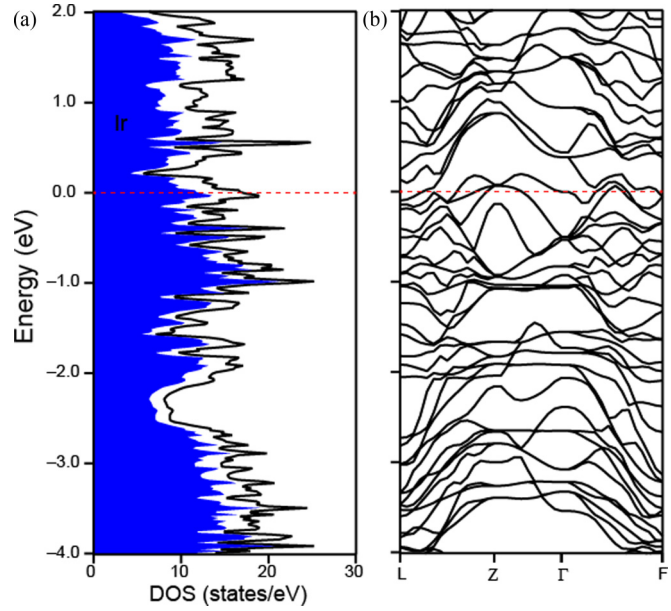

FIG. 10. (a) Partial DOS of Ir and Nd in $NdIr_3$ obtained by treating the $4f$ electrons on Nd as core electrons. (b) The band structure of $NdIr_3$. The red dashed line represents the Fermi level. The blue shading in panel (a) represents the total contribution of the Ir valence states to the DOS.

not shift with applied magnetic field (red solid line, inset Fig. 8) suggesting little magnetic character to the transition. Therefore, we suggest that the high-temperature anomaly may be related to electronic instabilities such as a CDW [79–81]. However, in order to properly determine the nature of the 70 K transition, further study is necessary.

Figure 9 presents the electrical resistivity of $NdIr_3$ at low temperatures measured in the vicinity of the transition. For $\mu_0 H = 0$ T the magnetic phase transition manifests itself as a small drop below $T_C \sim 11$ K. With lowering temperature the plotted $\rho(T)$ curve decreases first more rapidly due to the reduction of magnetic disorder scattering, and then reaches an almost constant value attributed to the residual resistivity ρ_0. The residual resistivity ratio, defined as $RRR = \rho(300\,\mathrm{K})/\rho(15\,\mathrm{K})$, is about 1.5. The low value of RRR may either simply originate from the polycrystalline form of the sample or be caused by possible internal disorder at a level that is below the detection limit for our x-ray-diffraction technique. The same figure depicts the low-temperature part of the electrical resistivity of $NdIr_3$ in applied magnetic fields up to 3 T. The resistivity slightly decreases with the application of magnetic fields in the entire temperature range studied. The magnetic transition anomaly is clearly affected by the magnetic field and fully suppressed by the highest applied field of 3 T. The inset of Fig. 9 shows $d\rho/dT$ versus temperature in the vicinity of the magnetic transition. The transition temperature determined as the maximum of $d\rho/dT$ is equal to 10.6 K under zero magnetic field in agreement with the temperature obtained from the magnetic susceptibility and heat-capacity measurements.

To further understand the electronic structure of $NdIr_3$, we performed electronic DOS and band-structure calculations (see Fig. 10). When treating the Nd $4f$ electrons as valence electrons, in variance with convention for rare-earth intermetallics, the calculations do not converge [50]. Thus, we treated the $4f$ electrons on Nd as core electrons. The DOS and band structure provide insight into the physical properties of the material, including the metallic properties, due to the continuous DOS across the Fermi level. The $6s$ and $5d$ electrons on Ir are highly hybridized with 6s electrons on Nd. After applying spin polarization, no magnetic moment was observed, which indicates that the magnetic moments in $NdIr_3$ arise solely from the $4f$ electrons on the Nd atoms.

IV. SUMMARY

We have synthesized a polycrystalline sample of the binary compound $NdIr_3$, and studied its magnetic, transport, and thermal properties. In contrast to one of the previous reports but in agreement with another [52], powder x-ray diffraction shows that $NdIr_3$ belongs to the $RE_{2m+n}T_{4m+5n}$ structure series with $m = 1$ and $n = 1$ (space group $R\text{-}3m$) with refined lattice parameters $a = 5.3287(1)$ Å and $c = 26.2218(3)$ Å at room temperature. Detailed analysis of the temperature- and field-dependent magnetic susceptibility, specific-heat, and electrical resistivity measurements allowed us to observe anomalies around 11 and 70 K, indicating the occurrence

of phase transitions at those temperatures. The origin of the high-temperature anomaly is unknown, but the lack of thermal hysteresis suggests that it is a second-order phase transition.

At low temperature, the heat-capacity measurement of $NdIr_3$ shows a clear λ-like anomaly, which is attributed to a second-order phase transition of magnetic origin. The magnetic and transport measurements are consistent with a ferromagnetic ordering at $T_C \sim 10.6$ K. The value of observed specific-heat jump $\Delta C_p = 11.7\,\mathrm{J\,mol^{-1}K^{-1}}$ is very close to the expected value $\Delta C_p = 12.5\,\mathrm{J\,mol^{-1}K^{-1}}$ for a $J = 1/2$ Heisenberg system and indicates that the CEF likely removes the spin degeneracy and leaves the Nd ions in a doublet ground state. This scenario is also supported by the $R\ln 2$ entropy value observed at T_C.

It is worth noting that ferromagnetism in rare-earth intermetallic compounds is not often observed [82]. The present material is, however, rich in the $5d$ element Ir, which has strong spin-orbit coupling, and hence detailed studies of the $NdIr_3$ magnetic structure are of great interest.

ACKNOWLEDGMENTS

This work was supported by the Ministry of Science and Higher Education (Poland) under Project No. DI2016 020546 ("Diamentowy Grant"). The materials synthesis and powder x-ray-diffraction work at Princeton University was supported by the US Department of Energy, Division of Basic Energy Sciences, Grant No. DE-FG02-98ER45706. W.X. is supported by the Beckman Young Investigator Program.

[1] Y. Liu, H. Pan, M. Gao, and Q. Wang, J. Mater. Chem. **21**, 4743 (2011).
[2] C. C. Hsieh, H. W. Chang, X. G. Zhao, A. C. Sun, and W. C. Chang, J. Appl. Phys. **109**, 07A730 (2011).
[3] Y. Li, J. Shen, and Y. Chen, Solid State Sci. **12**, 33 (2010).
[4] E. Akiba, H. Hayakawa, and T. Kohno, J. Alloys Compd. **408**, 280 (2006).
[5] S. Yasuoka, Y. Magari, T. Murata, T. Tanaka, J. Ishida, H. Nakamura, T. Nohma, M. Kihara, Y. Baba, and H. Teraoka, J. Power Sources **156**, 662 (2006).
[6] J.-C. Crivello, J. Zhang, and M. Latroche, J. Phys. Chem. C **115**, 25470 (2011).
[7] K. H. J. Buschow, Rep. Prog. Phys. **40**, 1179 (1977).
[8] E. Talik, J. Heimann, J. Szade, and A. Chełkowski, J. Common Met. **155**, 241 (1989).
[9] E. Talik, J. Szade, J. Heimann, A. Winiarska, A. Winiarski, and A. Chełkowski, J. Common Met. **138**, 129 (1988).
[10] N. V. Tristan, K. Nenkov, T. Palewski, K. P. Skokov, and S. A. Nikitin, Phys. Status Solidi A **196**, 325 (2003).
[11] A. E. Teplykh, A. N. Pirogov, and N. V. Baranov, Mater. Sci. Forum **321**, 653 (2000).
[12] D. Gignoux, R. Lemaire, and D. Paccard, Solid State Commun. **8**, 391 (1970).
[13] Z. Fisk and A. C. Lawson, Solid State Commun. **13**, 277 (1973).
[14] J. Strychalska, M. Roman, Z. Sobczak, B. Wiendlocha, M. J. Winiarski, F. Ronning, and T. Klimczuk, Phys. C Supercond. Its Appl. **528**, 73 (2016).
[15] T. H. Geballe, B. T. Matthias, V. B. Compton, E. Corenzwit, G. W. Hull, and L. D. Longinotti, Phys. Rev. **137**, A119 (1965).
[16] H. Sugawara, H. Sato, T. Yamazaki, N. Kimura, R. Settai, and Y. Ōnuke, J. Phys. Soc. Jpn. **64**, 4849 (1995).
[17] S. B. Roy and P. Chaddah, Phys. Rev. B **55**, 11100 (1997).
[18] M. Wilhelm and B. Hillenbrand, Physica **55**, 608 (1971).
[19] S. B. Roy and B. R. Coles, Phys. B: Condens. Matter **163**, 424 (1990).
[20] V. B. Compton and B. T. Matthias, Acta Crystallogr. **12**, 651 (1959).
[21] B. T. Matthias, H. Suhl, and E. Corenzwit, Phys. Rev. Lett. **1**, 92 (1958).
[22] F.. Parker and H. Oesterreicher, J. Common Met. **90**, 127 (1983).
[23] I. S. Dubenko, R. Z. Levitin, A. S. Markosyan, A. B. Petropavlovsky, and V. V. Snegirev, J. Magn. Magn. Mater. **90**, 715 (1990).
[24] R. Nakabayashi, Y. Tazuke, and S. Murayama, J. Phys. Soc. Jpn. **61**, 774 (1992).
[25] D. Gignoux, R. Lemaire, P. Molho, and F. Tasset, J. Magn. Magn. Mater. **15**, 289 (1980).
[26] R. A. McCurrie, G. P. Carswell, and J. B. O'Neill, J. Mater. Sci. **6**, 164 (1971).
[27] B. T. Matthias, H. Suhl, and E. Corenzwit, Phys. Rev. Lett. **1**, 449 (1958).
[28] D. Gignoux, D. Givord, and A. Del Moral, Solid State Commun. **19**, 891 (1976).
[29] V. Crisan, V. Popescu, A. Vernes, D. Andreica, I. Burda, S. Cristea, and V. Caciuc, J. Alloys Compd. **223**, 70 (1995).
[30] Y. Iwatake, N. L. Okamoto, K. Kishida, H. Inui, J. Ishida, T. Kai, and S. Yasuoka, Int. J. Hydrog. Energy **40**, 3023 (2015).
[31] E. Parthé and R. Lemaire, Acta Crystallogr. B **31**, 1879 (1975).
[32] D. T. Cromer and A. C. Larson, Acta Crystallogr. **12**, 855 (1959).
[33] Y. Khan, Acta Crystallogr. B **30**, 1533 (1974).
[34] O. Sologub, P. Salamakha, A. P. Gonçalves, H. Ipser, and M. Almeida, J. Alloys Compd. **373**, L5 (2004).
[35] K. S. V. L. Narasimhan, R. A. Butera, R. S. Craig, and W. E. Wallace, J. Solid State Chem. **9**, 267 (1974).
[36] K. H. J. Buschow, J. Common Met. **72**, 257 (1980).
[37] T. Abe, J. Phys. Soc. Jpn. **55**, 4003 (1986).
[38] K. H. J. Buschow, J. Common Met. **16**, 45 (1968).
[39] T. Goto, M. Yamaguchi, T. Kobayashi, and I. Yamamoto, Solid State Commun. **77**, 867 (1991).
[40] L. Cataldo, A. Lefèvre, F. Ducret, M.-T. Cohen-Adad, C. Allibert, and N. Valignat, J. Alloys Compd. **241**, 216 (1996).
[41] F. Givord and R. Lemaire, Solid State Commun. **9**, 341 (1971).
[42] N. Haldolaarachchige, L. Schoop, M. A. Khan, W. Huang, H. Ji, Kalani Hettiarachchilage, and D. P. Young, J. Phys.: Condens. Matter **29**, 475602 (2017).

[43] Y. J. Sato, A. Nakamura, Y. Shimizu, A. Maurya, Y. Homma, D. Li, F. Honda, and D. Aoki, J. Phys. Soc. Jpn. **87**, 053704 (2018).
[44] Z. Blazina, R. C. Mohanty, and A. Raman, *Intermediate Phases in Some Rare-Earth-Metal-Iridium Systems* (Southern University, Baton Rouge, LA, 1989).
[45] F. Y. Fradin, H. B. Radousky, N. J. Zaluzec, G. S. Knapp, and J. W. Downey, Mater. Res. Bull. **17**, 427 (1982).
[46] V. N. Yeremenko, V. G. Khorujaya, and P. S. Martsenyuk, J. Alloys Compd. **204**, 83 (1994).
[47] J. Rodríguez-Carvajal, Phys. B: Condens. Matter **192**, 55 (1993).
[48] G. Krier, O. Jepsen, A. Burkhardt, and O. K. Andersen, The TB-LMTO-ASA program, Stuttgart, April (1995).
[49] M. E. Casida, C. Jamorski, K. C. Casida, and D. R. Salahub, J. Chem. Phys. **108**, 4439 (1998).
[50] O. Jepsen and O. K. Andersen, Z. Phys. B: Condens. Matter **97**, 35 (1995).
[51] H. J. Monkhorst and J. D. Pack, Phys. Rev. B **13**, 5188 (1976).
[52] Y.-T. Ning, X.-M. Zhou, Y. Zhen, N.-Y. Chen, H. Xu, and J.-Z. Zhu, J. Common Met. **147**, 167 (1989).
[53] N. C. Popa and D. Balzar, J. Appl. Crystallogr. **41**, 615 (2008).
[54] J. Jensen and A. Mackintosh, *Rare Earth Magnetism: Structures and Excitations* (Clarendon Press, Oxford, 1991).
[55] T. T. M. Palstra, G. J. Nieuwenhuys, R. F. M. Vlastuin, J. van den Berg, J. A. Mydosh, and K. H. J. Buschow, J. Magn. Magn. Mater. **67**, 331 (1987).
[56] L. Salamakha, E. Bauer, G. Hilscher, H. Michor, O. Sologub, P. Rogl, and G. Giester, Inorg. Chem. **52**, 4185 (2013).
[57] L. Li, Y. Yi, K. Su, Y. Qi, D. Huo, and R. Pöttgen, J. Mater. Sci. **51**, 5421 (2016).
[58] S. Jia and R. J. Cava, Phys. Rev. B **82**, 180410 (2010).
[59] G. Cao, J. Bolivar, S. McCall, J. E. Crow, and R. P. Guertin, Phys. Rev. B **57**, R11039 (1998).
[60] V. I. Zaremba, D. Kaczorowski, G. P. Nychyporuk, U. C. Rodewald, and R. Pöttgen, Solid State Sci. **6**, 1301 (2004).
[61] K. Marumoto, F. Takayama, and Y. Miyako, J. Magn. Magn. Mater. **177**, 353 (1998).
[62] V. Goruganti, K. D. D. Rathnayaka, J. H. Ross, Y. Öner, C. S. Lue, and Y. K. Kuo, J. Appl. Phys. **103**, 073919 (2008).
[63] B. Barbara, D. Gignoux, and C. Vettier, *Lectures on Modern Magnetism* (Science Press, Beijing, 1988).
[64] A. Arrott, Phys. Rev. **108**, 1394 (1957).
[65] A. Arrott and J. E. Noakes, Phys. Rev. Lett. **19**, 786 (1967).
[66] A. K. Pramanik and A. Banerjee, Phys. Rev. B **79**, 214426 (2009).
[67] Y. Takahashi, J. Phys.: Conf. Ser. **868**, 012002 (2017).
[68] Y. Takahashi, J. Phys.: Conf. Ser. **344**, 012002 (2012).
[69] J. Yang, B. Chen, H. Ohta, C. Michioka, K. Yoshimura, H. Wang, and M. Fang, Phys. Rev. B **83**, 134433 (2011).
[70] J. W. G. Bos, M. Lee, E. Morosan, H. W. Zandbergen, W. L. Lee, N. P. Ong, and R. J. Cava, Phys. Rev. B **74**, 184429 (2006).
[71] H. Kuwahara, Y. Tomioka, A. Asamitsu, Y. Moritomo, and Y. Tokura, Science **270**, 961 (1995).
[72] N. Ni, S. Nandi, A. Kreyssig, A. I. Goldman, E. D. Mun, S. L. Bud'ko, and P. C. Canfield, Phys. Rev. B **78**, 014523 (2008).
[73] V. N. Dmitrieva, T. N. Rezuhina, L. M. Vareha, V. D. Vorobiev, V. F. Domashev, B. A. Gusynin, L. I. Kravchenko, and V. A. Mel'nikova, Metallphysics, Republican Interdepartmental Digest **49**, 109 (1973) (in Russian).
[74] R. Tediosi, F. Carbone, A. B. Kuzmenko, J. Teyssier, D. van der Marel, and J. A. Mydosh, Phys. Rev. B **80**, 035107 (2009).
[75] S. Ramakrishnan, Curr. Sci. **88**, 96 (2005).
[76] F. Galli, S. Ramakrishnan, T. Taniguchi, G. J. Nieuwenhuys, J. A. Mydosh, S. Geupel, J. Lüdecke, and S. van Smaalen, Phys. Rev. Lett. **85**, 158 (2000).
[77] V. Zaremba, Y. Galadzhun, B. Belan, A. Pikul, J. Stępień-Damm, and D. Kaczorowski, J. Alloys Compd. **316**, 64 (2001).
[78] P. L. Rossiter, *The Electrical Resistivity of Metals and Compounds* (Cambridge University Press, New York, 1987).
[79] G. Grüner, Rev. Mod. Phys. **60**, 1129 (1988).
[80] N. Ru, C. L. Condron, G. Y. Margulis, K. Y. Shin, J. Laverock, S. B. Dugdale, M. F. Toney, and I. R. Fisher, Phys. Rev. B **77**, 035114 (2008).
[81] H. Yao, J. A. Robertson, E.-A. Kim, and S. A. Kivelson, Phys. Rev. B **74**, 245126 (2006).
[82] S. Ahamed, R. Moessner, and O. Erten, Phys. Rev. B **98**, 054420 (2018).